TUDelft

Delft University of Technology

Experimental evaluation of the mesh load factor (K 3) of a 6MW wind turbine gearbox

Santiago, Unai Gutierrez; Sisón, Alfredo Fernández; Polinder, Henk; Van Wingerden, Jan Willem

Important note
To cite this publication, please use the final published version (if applicable).
Please check the document version above.

PAPER • OPEN ACCESS

Experimental evaluation of the mesh load factor ($K\gamma$) of a 6MW wind turbine gearbox

To cite this article: Unai Gutierrez Santiago *et al* 2022 *J. Phys.: Conf. Ser.* **2265** 032003

View the article online for updates and enhancements.

Experimental evaluation of the mesh load factor (K_γ) of a 6MW wind turbine gearbox

Unai Gutierrez Santiago [1,2], Alfredo Fernández Sisón [2], Henk Polinder [1], Jan-Willem van Wingerden [1]

[1]TU Delft 3mE, Mekelweg 2, 2628 CD, Delft, The Netherlands.
[2]Siemens Gamesa Renewable Energy, Parque Tecnológico de Bizkaia, 48170 Zamudio, Spain.

E-mail: `u.gutierrezsantiago@tudelft.nl`

Abstract.   The significant increase in rotor diameters seen in modern wind turbines has pushed gearbox manufacturers to introduce technological innovations to increase the torque density of current designs. Driven by the need to lower the cost of energy from wind and size limitations imposed by logistic constraints in onshore wind, a trend has emerged to increase the number of planetary stages and the number of planet gears per stage. One of the main challenges of next-generation gearbox designs is sharing the load evenly between a high number of planets. This paper presents an experimental evaluation of the mesh load factor of a modern 6MW wind turbine gearbox with five planets in the first planetary stage. Results from the traditional method, based on tooth root strain gauges, and from strain measurements in the outer surface of the ring gear are described and assessed. Both experimental approaches have yielded lower mesh load factor values than the default values required in the standard "Design requirements for wind turbine gearboxes" IEC 61400-4. Since the mesh load factor is used for gear rating and sizing, a lower value allows a more optimized gearbox design, which leads to a significant improvement in torque density and cost.

1. Introduction
Reducing the cost of energy (CoE) has become one of the main research drivers in Wind Energy [1]. As a result, wind turbines have experienced an astonishing increase in rotor diameter. In the overall breakdown of costs of onshore wind, the gearbox is one of the main contributors due to the associated capital expenditure and the considerable impact on operation and maintenance costs [2]. In this context, gearbox manufacturers have striven to reduce the cost of gearboxes by increasing the torque density of modern designs. Multiple technological innovations have been introduced, e.g., new materials, improved manufacturing tolerances, and additional surface finishing techniques. However, increasing the number of planetary stages and the number of planet gears in each stage are the two most promising avenues to increase the torque density and keep the gearbox diameter within the limitations imposed by logistic constraints [3]. One of the main challenges of next-generation gearbox designs is sharing the load evenly between the high number of planets. The load-sharing behavior of planetary gears has been extensively studied in the literature. Kahraman et al. researched its dependency on manufacturing errors and the associated dynamic effects [4] and presented an experimental study in [5]. Singh, A. proposed an analytical formulation for the relationship between planet load sharing behavior and positional errors [6]. These studies were conducted on smaller module gears for automotive or

helicopter applications. Guo, Y. and Keller, J. generalized this analytical formulation for wind turbine gearboxes with a three-planet, floating epicyclic configuration [7, 8]. New analytical tools are needed to predict the load-sharing behavior in modern wind turbine gearboxes with more planets. These tools need to be demonstrated and validated through experimental evaluation.

For split path gear meshes, the gear rating standard ISO 6336-1 [9] defines the mesh load factor K_γ as the quotient between the highest load carried by a single path divided by the average load. In planetary gear stages, this corresponds to the highest load carried by a single planet divided by the average load of all planets. Design requirements for wind turbine gearboxes are set by the standard IEC 61400 – 4 [10]. This standard specifies default values of the load mesh factor K_γ as a function of the number of planets. These default values are given in Table 1.

Table 1. Mesh load factor K_γ for planetary stages according to IEC 61400-4.

| Number of planets	3	4	5	6	7
Mesh load factor K_γ	1.10	1.25	1.35	1.44	1.47

For a high number of planets, the mesh load factors presented in Table 1 are conservative and would lead to gearbox designs with poor torque density values. The standard allows lower mesh load factor values if they are demonstrated by gear teeth root strain gauge measurements during prototype testing. Performing such tooth root strain measurements is complex and expensive. A recently developed method to measure torque using fiber optic strain sensors on the outer surface of the ring gear [11] has proven to provide additional information about the way torque is shared by the different planets.

The main contribution of this study is to perform an experimental evaluation of the mesh load factor (K_γ) of a five-planet first planetary stage from a modern 6MW wind turbine gearbox. The traditional method to evaluate the mesh load factor based on strain gauge measurements in the gear teeth roots has been compared against values obtained from the strain measurements on the outer surface of the ring gear to assess the new method. The results from both approaches have been compared to the requirements set by the standard IEC 61400 – 4 [10].

The remainder of this paper is organized as follows, Section 2 describes the experimental procedure used to evaluate the mesh load factor K_γ. Section 2.1 covers the traditional method based on tooth root strain measurements, and Section 2.2 describes the method based on strain measurements on the outer surface of the ring gear using fiber optic sensors. Section 3 discusses the results obtained with both signal processing procedures, and Section 4 draws the main conclusions of this work and suggests recommendations for future work.

2. Experimental evaluation of the mesh load factor K_γ

This study was conducted using a Siemens Gamesa Renewable Energy (SGRE) gearbox manufactured by Gamesa Energy Transmission (GET). The gearbox is a 3 stage gearbox, where the first and second are epicyclic planetary stages, and the third is a parallel stage. The first planetary has five planets and the second stage has three. The rated power of the gearbox is 6MW and weights approximately 44000Kg. A full-scale prototype gearbox, instrumented with strain gauges in two roots of the sun gear and fiber optical strain sensors on the outer surface of the ring gear, was tested in a back-to-back test bench up to 100% of its nominal torque. The first stage of this gearbox was chosen for this study because it is representative of current gearbox designs. With five planets, it provides a suitable case to evaluate the requirements of standard IEC 61400 - 4. All tests presented in this study were performed on the back-to-back test bench shown in Fig. 1, property of the company DMT GmbH & Co. KG [12] at Krefeld (Germany) with electric motors of rated power of 7.5 MW.
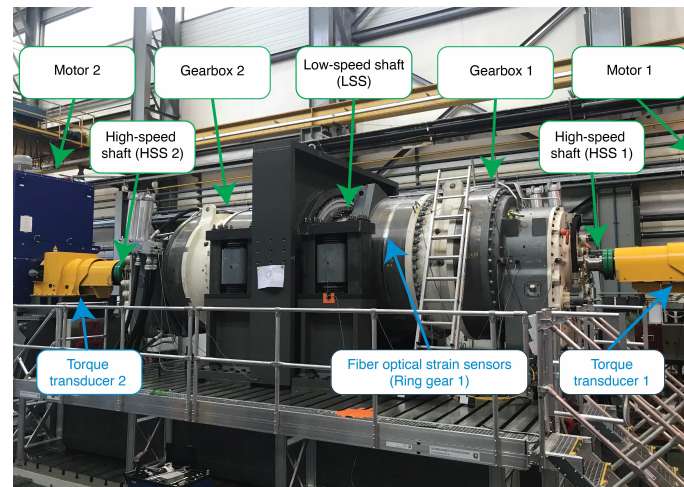
Figure 1. SGRE gearboxes on a back-to-back test bench (property of DMT GmbH & Co. KG).

### 2.1. Load mesh factor from sun gear root instrumentation

The traditional method to evaluate the mesh load factor is based on measurements from strain gauges installed in the gear tooth root. According to the standard IEC 61400 – 4 [10] these strain gauges are a compulsory part of the verification process of a new gearbox design and also serve to evaluate the gear mesh contact patterns and the load intensity distribution along the face width of the gears (K_β). The measurement system was comprehensively described in [13]. However, it is worth emphasizing two critical items of the instrumentation:

- Location of strain gauges in the gear root: When a gear tooth is subjected to the mesh force as depicted in Figure 2, where α is the pressure angle. According to the standard ISO 6336 [9] the highest stresses can be found in the sections defined by the 30 degree tangents. In theory, these spots of maximum stress would lead to the highest possible signal-to-noise ratio. However, these spots also exhibit large stress gradients, making them very sensitive to positioning errors. In practice, the middle section between teeth offers a more suitable location to place the strain gauges. The strains are large enough to give good readings, and the smaller stress gradient reduces the sensitivity to positioning errors. Additionally, the middle section offers more clearance with the mating tooth, which eases the physical installation process of the gauges and associated wiring.

- Number of strain gauges along the gear face width: The number of gauges to be installed along the face width in each root is a compromise between the required spatial resolution and the time and cost of the installation. In wind turbine gearboxes, considering the typical gear dimensions and the ratio of face width to the normal module, a number of 8 strain gauges has been found to produce satisfactory results. Figure 3 shows how these eight gauges were distributed along a tooth root of the sun. This root was arbitrarily labeled as root number 1. The tooth root number 13, in the rotor's clockwise direction, was also instrumented in the same way for redundancy purposes.

The sun gear is a rotating part, and therefore, a special data acquisition system is needed. For the present study, bespoke uniaxial strain gauges together with gear alignment electronic modules developed by JR Transmission Dynamics [14] were used. These modules provide strain gauge conditioning using a Wheatstone bridge with a quarter bridge configuration; they are equipped with 8-channel synchronous acquisition and low-noise 12 bit analog to digital converters. Once the data is logged, a Bluetooth system transmits the data wirelessly. In this
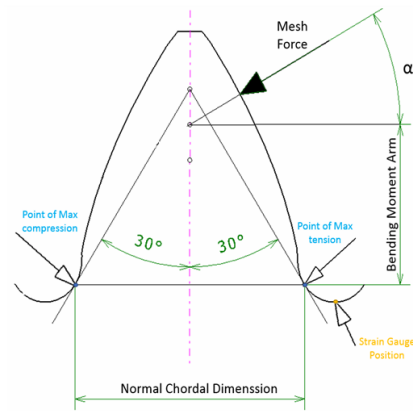
Figure 2. Strain gauge positioning in the gear tooth root.
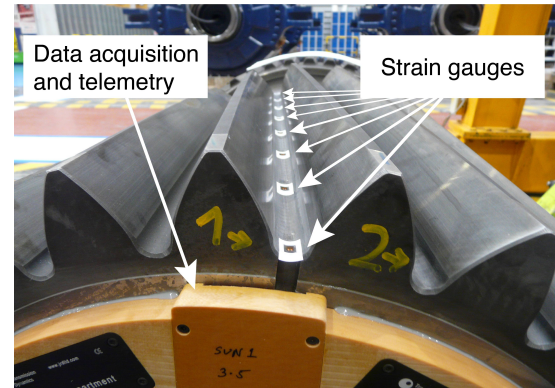
Figure 3. Strain gauge placement on a root of a sun gear.

study, two roots (arbitrarily numbered 1 and 13) were instrumented with eight strain gauges on each root connected to independent 8-channel modules. Part of the electronic module can be seen in Fig. 3. This picture was taken before soldering the wires from the strain gauges to the electronic module.

In the case of the sun gear, the instrumented gear tooth will mesh with all the planets allowing the mesh load factor (K_γ) to be evaluated by comparing the mesh intensity of the gear meshes with the different planets. For each revolution of the sun relative to the carrier, a number of meshing cycles equal to the number of planets are observed in the time waveform of the strain gauges located in a tooth root of the sun gear. Figure 4 shows the raw data recorded from the eight strain gauges of the root number 1 of the sun. A once-per-revolution tachometer signal was also logged synchronously to identify the angular position of the sun relative to the carrier. The sun gear acts as a driven gear in the mesh with the planets. Therefore, during the start of the mesh cycle, when the tooth before the instrumented root is loaded, the strain gauge first observes a positive strain or traction. As the meshing cycle continues, the strain gauges will undergo compression or negative strain once the following tooth after the instrumented root becomes loaded.

The peak-to-peak strain value of the traction-compression cycle observed during the mesh cycle was chosen to measure the relative root stress of each strain gauge. Figure 5 shows the normalized peak-to-peak values of each strain gauge for the five mesh events of a single revolution of the sun gear relative to the carrier. The relative strain values are plotted against the axial position along the width of the sun gear shown in Fig. 3. The rotor side corresponds to the left part of the graph and the generator side to the right. From the strain distributions shown in Fig. 5, the area below each strain distribution was chosen as the mesh intensity value assigned to each gear mesh. This mesh intensity, denoted as i_{mesh}, can be computed using the following equation and was :

$$i_{mesh} = \sum_{n=1}^{N} b_n \Delta\delta_{n,mesh} \tag{1}$$

where b_n is the length of face width covered by the strain gauge n and $\Delta\delta_{n,mesh}$ is the peak-to-peak strain measured by the strain gauge n during the mesh event. N is the total number of strain gauges placed along the face width. If we have P number of planets, then, for a given
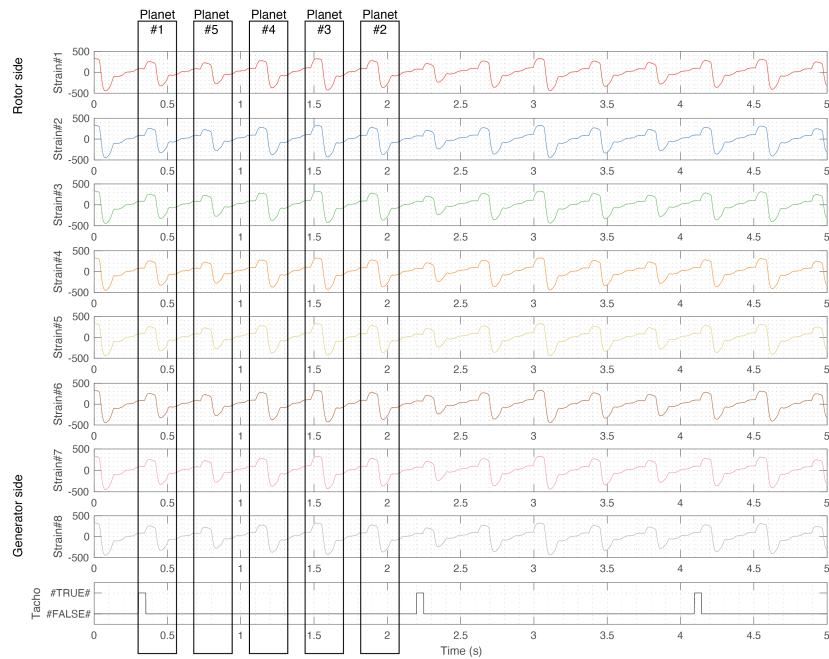
Figure 4. Strain signals of all 8 root gauges and once-per-revolution tachometer.

revolution rev of the sun relative to the carrier the following mesh intensities can be computed: $i_{1,rev}, i_{2,rev}, i_{3,rev}, ..., i_{P,rev}$.

A mesh load factor for a single revolution can be evaluated by comparing all the mesh intensity values of a single revolution and dividing the maximum mesh intensity from a single planet by the average of all planets (see Eq. 2). Since dynamic effects can influence the different mesh
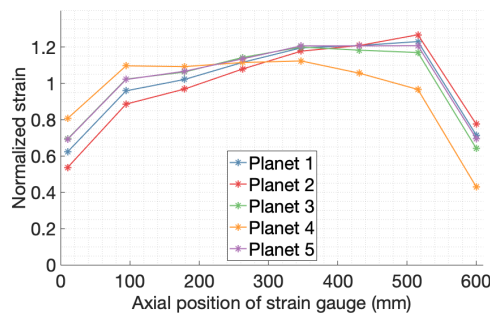
Figure 5. Root strain distribution for the mesh events of a single revolution of the sun relative to the carrier.
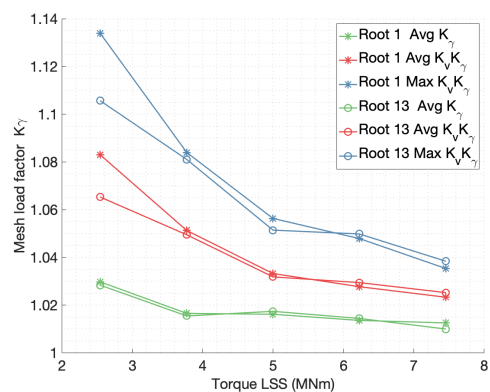
Figure 6. Mesh load factors obtained from strain measurements in two roots of the sun gear.

intensity values during a complete revolution, this value has been denoted as $K_v K_{\gamma rev}$:

$$K_v K_{\gamma rev} = \frac{max(i_{1,rev}, i_{2,rev}, i_{3,rev}, ..., i_{P,rev})}{\frac{\sum_{p=1}^{P} i_{p,rev}}{P}} \qquad (2)$$

The term $K_v K_\gamma$ is a loose interpretation of the standard ISO 6336 [9]. A method to measure the dynamic effects covered by K_v is unavailable in the industry. The authors understand that the dynamic effects influence the mesh intensity measurements within a revolution because the mesh events were measured at different time instants. However, it cannot be guaranteed that all the dynamic effects will show in the few mesh events recorded by the instrumented tooth.

In the present study, the tooth root strains were recorded for tests performed with 33, 50, 67, 83 and 100% of the nominal torque. During each test, the reference torque command was kept stationary. Around 20 revolutions of the sun relative to the carrier were recorded for each test. Throughout these revolutions, the strain distribution was observed to change dynamically. The $K_v K_\gamma$ values were computed for all the recorded revolutions. The average $K_v K_\gamma$ and the worst case or maximum $K_v K_\gamma$ were selected. A third value relative to the mesh load factor was explored. The peak-to-peak strain data of each strain gauge was averaged, taking into account the planet that produced the gear mesh. This average distribution filters out the contributions of K_v assuming that the dynamic effects covered by the factor K_v are uncorrelated with the mesh load factor K_γ and that the recorded data covers enough revolutions. This average mesh load factor has been denoted as $K_{\gamma,avg}$:

$$K_{\gamma,avg} = \frac{max(i_{1,avg}, i_{2,avg}, i_{3,avg}, ..., i_{p,avg})}{\frac{\sum_{p=1}^{P} i_{p,avg}}{P}} \qquad (3)$$

where the i_{pavg} is the average mesh intensity produced by the planet p which be computed using the following equation:

$$i_{p,avg} = \frac{\sum_{r=1}^{R} i_{p,r}}{R} \qquad (4)$$

Figure 6 shows the average K_γ, average $K_v K_\gamma$ and maximum $K_v K_\gamma$ results of both instrumented roots (roots number 1 and 13) obtained during the tests performed with stationary torque values of 33, 50, 67, 83 and 100% of the nominal torque.

2.2. Load mesh factor from ring gear outer surface instrumentation

A new method to measure the input torque of wind turbine gearboxes was introduced in [11]. This method is based on strain measurements on the outer surface of the ring gear. The instrumentation requirements and the data logging process are simplified because the ring gear is static. Optical strain sensors based on fiber Bragg gratings (FBGs) were used because they offer a higher signal-to-noise ratio and are immune to electromagnetic interference. Since multiple strain sensors can be accommodated in a single fiber, they also allow a more straightforward installation. A satisfactory correlation was found between the input torque of the carrier and the deformations on the outer surface. Furthermore, the procedure based on peak-to-peak strain values provided information about the load sharing between planets.

Four optical fibers were installed on the outer surface of the first stage ring gear, at the middle section along the width of the ring gear in the axial direction, as shown in Fig. 1. The fibers were installed tangentially to the middle section, covering a complete revolution along the outer perimeter of the ring gear. Figure 7 shows the radial and angular location of all the strain sensors with the corresponding labels in a rotor side section view. The four different colors of

the sensor labels indicate how the FBGs belong to separate fibers (S01 to S15 in fiber number 1, S16 to S28 in fiber number 2, S29 to S41 in fiber number 3, and S42 to S54 in fiber number 4). The fiber optical sensors were supplied and installed by the company Sensing360 B.V. [15]. A more comprehensive description of the optical fiber instrumentation used can be found in [11].
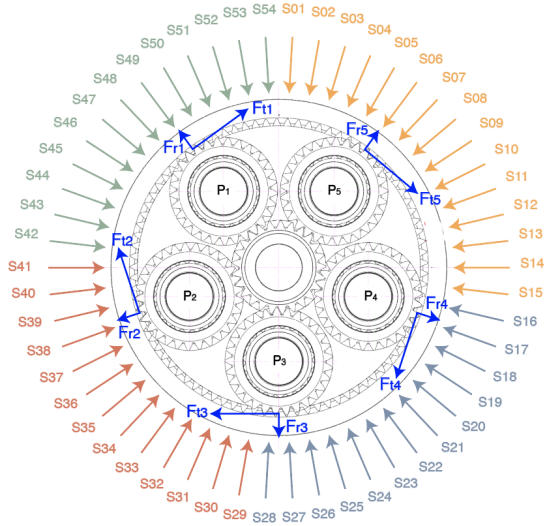
Figure 7. Location of the fiber optical strain sensors (S01 to S54).
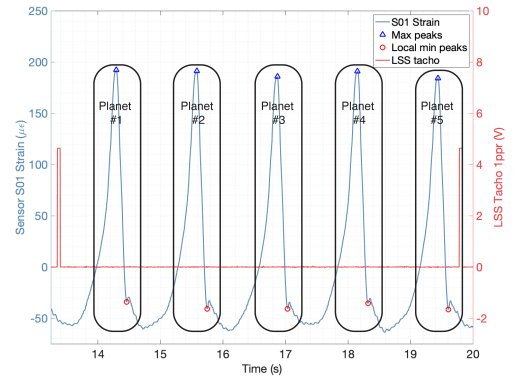
Figure 8. Sensor S01 Strain signal (left axis) during a single revolution of the input shaft (right axis) with detected peaks assigned to the corresponding planet.

Fiber Bragg gratings are sensitive to strain and temperature. The signals were detrended to remove the effect of temperature on the measured shifts in wavelengths of the FBGs. Once the long-term shift caused by temperature had been removed, the remaining signal was considered to be caused entirely by the strain imposed from the planet gear mesh events. A correlation between the average torque and the average peak-to-peak values of the strain sensors placed on the ring gear's outer surface was found in [11]. An inductive sensor was used to provide a pulse for every full rotation of the input shaft so that the relative position of the planet carrier is known and peak-to-peak values can be assigned to individual planets as shown in Fig. 8. For every revolution of the carrier, a value of $K_v K_\gamma$ can be computed using the peak-to-peak values as $i_m esh$ in Eq. 2. Similarly, the following expression is proposed to derive the average $K_{\gamma,p}$ of a particular planet:

$$K_{\gamma,p} = \frac{\overline{\Delta \delta_p}}{\overline{\Delta \delta_{all}}}, \tag{5}$$

where $\overline{\Delta \delta_p}$ is the average peak-to-peak strain value measured from all mesh events caused by a particular planet p, and $\overline{\Delta \delta_{all}}$ is the average peak-to-peak value of all planets. In the instrumentation set-up used for this study, the number of strain sensors on the ring gear is not an integer multiple of the number of planets, therefore, it is not possible to compare strain peaks in different positions simultaneously. Figure 9 shows the resulting average K_γ for each strain sensor position for a test conducted at 100% of torque.

Short tests under 19 different stationary speed and torque conditions were performed to characterize the relationship between torque and the mesh load factor. The torque level was increased in five percent increments from 10 to 100 % of the nominal torque. For each test, strain data was recorded for around 35 revolutions of the carrier. The gearbox rotational speed was kept constant and equal to the nominal value. Figure 10 shows the average K_γ values of

the five planets against torque. The values shown by the circular markers in Fig. 10 represent the mean value of all 54 sensors, and the shaded patches represent the bounds limited by the minimum and maximum K_γ.
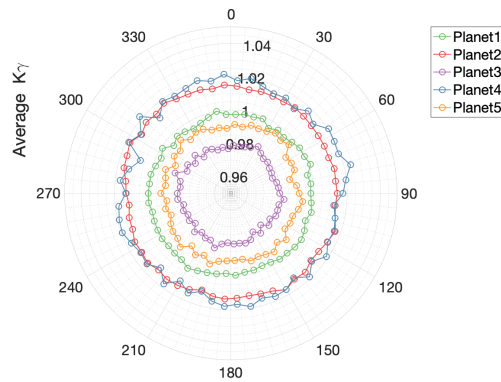
**Figure 9.** Average K_γ per planet for each sensor evaluated at 100% nominal torque.
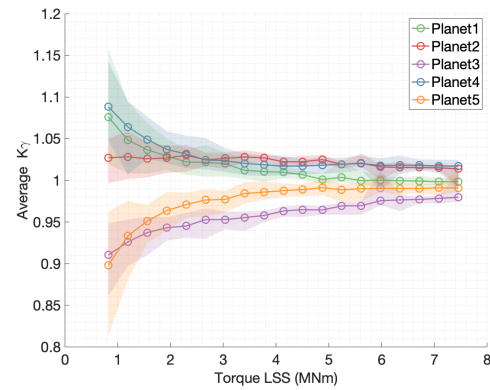
Figure 10. $K_{\gamma,avg}$ values from all fiber strain sensors, the mean value is represented by the circular marker and the min-max bounds by the shaded patch.

3. Discussion of results

This section will discuss the main findings gathered through the experimental evaluation of the mesh load factor K_γ of the first planetary stage from a modern 6MW wind turbine gearbox. Two alternative approaches have been studied. First, the traditional method based on gear tooth root strain measurements has been described in Section 2.1. Then a different approach based on strain measurements on the outer ring gear using optic fiber sensors has been presented in Section 2.2. The results from both experimental approaches have been combined in Fig. 11. The comparison has been made for the three mesh load factors defined in Section 2, i.e., average $K_v K_\gamma$, maximum $K_v K_\gamma$ and average K_γ. In the case of the fiber-optic strain sensors the triangular marker represents the mean value of all sensors and the shaded patch the minimum to maximum bounds. As it can be seen, both approaches yield similar results and a good fit has been found between the different K_γ values obtained.

It is worth noticing that results from the gear tooth root instrumentation were produced for test conditions with 33, 50, 67, 83 and 100% of the nominal torque. On the other hand, using the strain sensors on the outer surface of the ring gear, the mesh load factor could be evaluated for 19 short tests from 10 to 100 % of the nominal torque in five percent increments. This is because measuring in the static frame overcomes the main drawbacks of data transfer from rotating components and makes data gathering less time-consuming. Therefore more test conditions could be performed in a shorter time.

Both measurement approaches show an improvement of the mesh load factor with torque. This is expected because of the flexibility of the gearbox components. As torque increases, the deformation of these components increases, reducing the influence of manufacturing errors and better load sharing is achieved. The fit between the two approaches is best from 66 to 100% of the nominal torque. The sun gear results seem to be more sensitive to torque for lower torque values and show a larger increase when torque is reduced. However, the torque region below 33% was not recorded with the sun gear instrumentation, and a direct comparison was not possible for such low torque levels. Low torque levels are not critical for gear rating and life expectations,
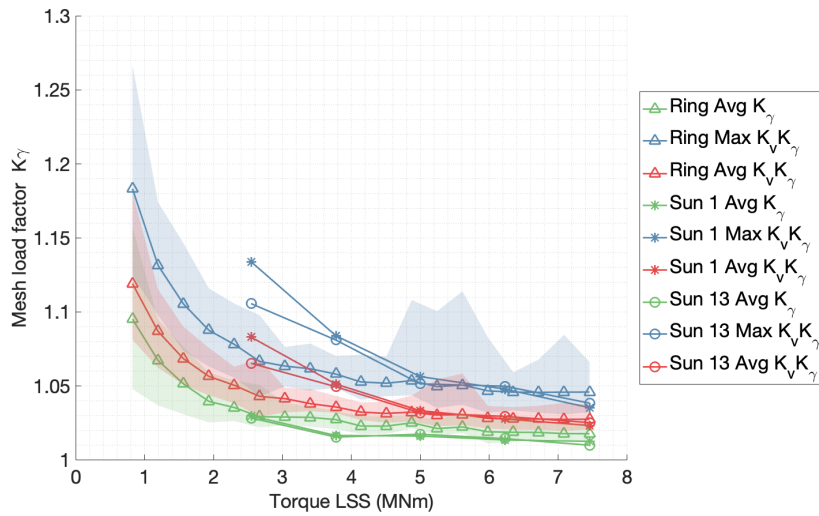
Figure 11. Average K_γ, maximum $K_v K_\gamma$ and average $K_v K_\gamma$ values evaluated from tooth root strain measurements at the sun gear, denoted as Sun1 and Sun13, compared with values evaluated from strain sensors on the ring, denoted as Ring.

and therefore having high mesh load factors at lower torque values is not a concern for gearbox manufacturers.

The experimental mesh load factor K_γ results for the nominal working condition of the gearbox are significantly lower than the default values required by the standard IEC 61400-4 [10] shown in Table 1. Care must be taken when interpreting these results because the results presented in this study come from a single instrumented gearbox. Therefore, the manufacturing class and accuracy of the serial production gearbox components shall be controlled so that the behavior of the prototype is representative of the complete fleet. Moreover, with the instrumentation set-up presented in this study, an instantaneous mesh load factor could not be evaluated. The average mesh load factor seems appropriate for gear rating and life calculations, but the instantaneous behavior of load-sharing between planets remains to be researched. The present study is based on measurements taken on a gearbox back-to-back test bench where only torque and speed can be controlled. The effects of non-torque loads, i.e., axial forces and bending moments, need to be researched to fully demonstrate these findings in a wind turbine installation.

4. Conclusions

The present study has shown that the fiber optical strain measurements in the outer surface of the ring gear yield equivalent mesh load factor K_γ results compared to the traditional method based on strain gauges located in the roots of the sun gear teeth. This is a promising result because transferring the resulting signal from the rotating sun and powering the data acquisition devices is difficult and costly. Measuring in the static ring gear overcomes these drawbacks allowing a more straightforward installation and easing the data recording requirements for testing.

The experimental mesh load factor K_γ results obtained for a modern 6MW wind turbine gearbox with five planets in the first stage are significantly lower than the default values required by the standard IEC 61400-4 [10]. Since K_γ is directly used for gear rating and life calculations, a low value of K_γ allows for a more optimized gearbox design, and therefore significant improvements in torque density are expected. The manufacturing class of the gears and the

accuracy of the serial production gearbox components have to be controlled to extrapolate the results obtained from a single prototype to the entire fleet.

For future work, researching the instantaneous load-sharing behavior between planets is suggested. The placement of the strain sensors used in the instrumentation set-up of this study does not allow evaluating simultaneous mesh events. However, the authors believe this could be overcome with improved sensor placement.

References

[1] van Kuik G A M, Peinke J, Nijssen R, Lekou D, Mann J, Sørensen J N, Ferreira C, van Wingerden J W, Schlipf D, Gebraad P, Polinder H, Abrahamsen A, van Bussel G J W, Sørensen J D, Tavner P, Bottasso C L, Muskulus M, Matha D, Lindeboom H J, Degraer S, Kramer O, Lehnhoff S, Sonnenschein M, Sørensen P E, Künneke R W, Morthorst P E and Skytte K 2016 Long-term research challenges in wind energy – a research agenda by the european academy of wind energy *Wind Energy Science* **1** 1–39 , `https://wes.copernicus.org/articles/1/1/2016/`

[2] Stehly T, Beiter P, Heimiller D and Scott G 2018 2017 cost of wind energy review , `https://www.nrel.gov/docs/fy18osti/72167.pdf`

[3] Nejad A R, Keller J, Guo Y, Sheng S, Polinder H, Watson S, Dong J, Qin Z, Ebrahimi A, Schelenz R, Guzmán F G, Cornel D, Golafshan R, Jacobs G, Blockmans B, Bosmans J, Pluymers B, Carroll J, Koukoura S, Hart E, McDonald A, Natarajan A, Torsvik J, Moghadam F K, Daems P J, Verstraeten T, Peeters C and Helsen J 2021 Wind turbine drivetrains: state-of-the-art technologies and future development trends *Wind Energy Science Discussions* **2021** 1–35 , `https://wes.copernicus.org/preprints/wes-2021-63/`

[4] Bodas A and Kahraman A 2004 Influence of Carrier and Gear Manufacturing Errors on the Static Load Sharing Behavior of Planetary Gear Sets *JSME International Journal Series C* **47** 908–915

[5] Ligata H, Kahraman A and Singh A 2008 An Experimental Study of the Influence of Manufacturing Errors on the Planetary Gear Stresses and Planet Load Sharing *Journal of Mechanical Design* **130** ISSN 1050-0472 041701 , `https://doi.org/10.1115/1.2885194`

[6] Singh A 2010 Load sharing behavior in epicyclic gears: Physical explanation and generalized formulation *Mechanism and Machine Theory* **45** 511–530 ISSN 0094-114X , `https://www.sciencedirect.com/science/article/pii/S0094114X09001931`

[7] Keller J, Guo Y, Zhang Z and Lucas D 2018 Comparison of planetary bearing load-sharing characteristics in wind turbine gearboxes *Wind Energy Science* **3** 947–960 , `https://wes.copernicus.org/articles/3/947/2018/`

[8] Guo Y and Keller J 2020 Validation of a generalized formulation for load-sharing behavior in epicyclic gears for wind turbines: Preprint , `https://www.osti.gov/biblio/1669557`

[9] ISO 2019 6336-1:2019 calculation of load capacity of spur and helical gears — part 1: Basic principles, introduction and general influence factors , `https://www.iso.org/standard/63819.html`

[10] ISO/IEC 2012 61400-4:2012 wind turbines — part 4: Design requirements for wind turbine gearboxes , `https://www.iso.org/standard/44298.html`

[11] Gutierrez Santiago U, Fernández Sisón A, Polinder H and van Wingerden J W 2021 Input torque measurements for wind turbine gearboxes using fiber optical strain sensors *Wind Energy Science Discussions* **2021** 1–28 , `https://wes.copernicus.org/preprints/wes-2021-69/`

[12] DMT-groupcom Dmt gmbh & co. kg Last accessed: 30 December 2021 , `https://www.dmt-group.com`

[13] Fernández Sisón A, Calvo Irisarri J, Olade Arce P and Gutierrez Santiago U Load intensity distribution factor evaluation from strain gauges at the gear root *Gear Solutions* , `https://gearsolutions.com/features/load-intensity-distribution-factor-evaluation-from-strain-gauges-at-the-gear-root/`

[14] http://wwwjrdltdcouk Jr dynamics limited Last accessed: 30 December 2021 , `http://www.jrdltd.co.uk`

[15] sensing360com Sensing 360 b.v. Last accessed: 30 April 2021 , `https://sensing360.com`